Journal of Power Sources 453 (2020) 227905

Contents lists available at ScienceDirect

Journal of Power Sources

journal homepage: www.elsevier.com/locate/jpowsour

A high rate performance positive composite electrode using a high P/S ratio and LiI composite solid electrolyte for an all-solid-state Li–S battery

Hiroshi Nagata [a,*], Yasuo Chikusa [b], Junji Akimoto [a]

[a] National Institute of Advanced Industrial Science and Technology (AIST), Central 5, 1-1-1 Higashi, Tsukuba, Ibaraki, 305-8565, Japan
[b] Nagase ChemteX Corporation, 236, Tatsunocho-nakai, Tatsuno, Hyogo, 679-4124, Japan

HIGHLIGHTS

- ▶ Ionic conductivity of high P/S ratio SEs was improved by LiI addition.
- ▶ $65Li_{1.6}PS_2{\cdot}35LiI$ showed ionic conductivity and high improvement effect of reactivity.
- ▶ Raising the temperature from 25 °C to 45 °C greatly improved the high rate performance.
- ▶ Discharge capacity of over 1000 $mAhg^{-1}$ was obtained at 25.5 mA cm^{-2} and 45 °C.

ARTICLE INFO

Keywords:
All-solid-state battery
Lithium–sulfur battery
Activation of sulfur
High energy density
High power density

ABSTRACT

All-solid-state lithium–sulfur batteries are believed to have sufficient energy density to be next-generation batteries. In manufacturing the batteries, it is necessary to improve the sulfur reactivity and ion conductivity in the positive electrode. In this study, we investigated $(100-x)(Li_{1.6}PS_2){\cdot}x(LiI)$ as a composite solid electrolyte with a high P/S ratio solid electrolyte and LiI to provide the dual functions of high sulfur activated property and high ionic conductivity. This solid electrolyte showed high ionic conductivity of over 0.5 mS cm^{-1} at over $x = 35$. The positive composite electrode using $65Li_{1.6}PS_2{\cdot}35LiI$ exhibited a good high rate capacity of over 1260 mA h g^{-1} (sulfur) at 6.4 mA cm^{-2} (0.8 C) and 25 °C. Furthermore, it showed excellent battery performance at 45 °C. The high rate capacity was 25.5 mA cm^{-2} (3.2 C) over 1000 mA h g^{-1}, and the 1 C cycle capacity was over 1230 mA h g^{-1} after 100 cycles.

1. Introduction

Rechargeable lithium-ion batteries are known to be high-performance energy storage devices and are widely used in many kinds of electronic gadgets. The use of lithium-ion battery devices is currently being explored for applications that require a high energy density, such as natural energy storage systems and electric vehicles. Currently, lithium-ion batteries do not satisfy these requirements due to the low theoretical energy density of the electrode active material used. Therefore, we focused on the lithium–sulfur (Li–S) battery, a sulfur positive active material that has an extremely high theoretical specific capacity of 1672 mA h g−1, which is higher than conventional lithium transition metal oxide positive active materials [1]. This paper shows the improvement of positive composite electrode performance of an all-solid-state Li–S battery using a solid electrolyte (SE) instead of an organic electrolyte. This system has several advantages, such as suppressing cycle degradation and improving safety, as it does not necessitate the use of a solvent with a high solubility of lithium polysulfide and low flash point [2,3]. At present, SEs are being actively investigated, and their ionic conductivity has been remarkably improved. Some show higher ionic conductivity than general liquid electrolytes [4,5] and it is expected that the battery performance of current lithium-ion batteries will be exceeded. However, sulfur shows low reactivity and capacity usage in positive electrodes due to its low electronic and ionic conductivity [6]. Therefore, it is necessary to include large amounts of electron conductive materials and SEs in the positive electrode, which shows a low energy density based on positive composite electrode weight. The comparison of the battery performance of several sulfur positive composite electrodes, including liquid systems, is summarized in the review article [7]. The comparison of battery performance in the positive electrode is based on the specific capacity (based on the sulfur weight). However, the battery performance

* Corresponding author.
E-mail addresses: nagata.hiroshi@aist.go.jp (H. Nagata), yasuo.chikusa@ncx.nagase.co.jp (Y. Chikusa), j.akimoto@aist.go.jp (J. Akimoto).

https://doi.org/10.1016/j.jpowsour.2020.227905
Received 12 January 2020; Received in revised form 12 February 2020; Accepted 14 February 2020
Available online 18 February 2020
0378-7753/

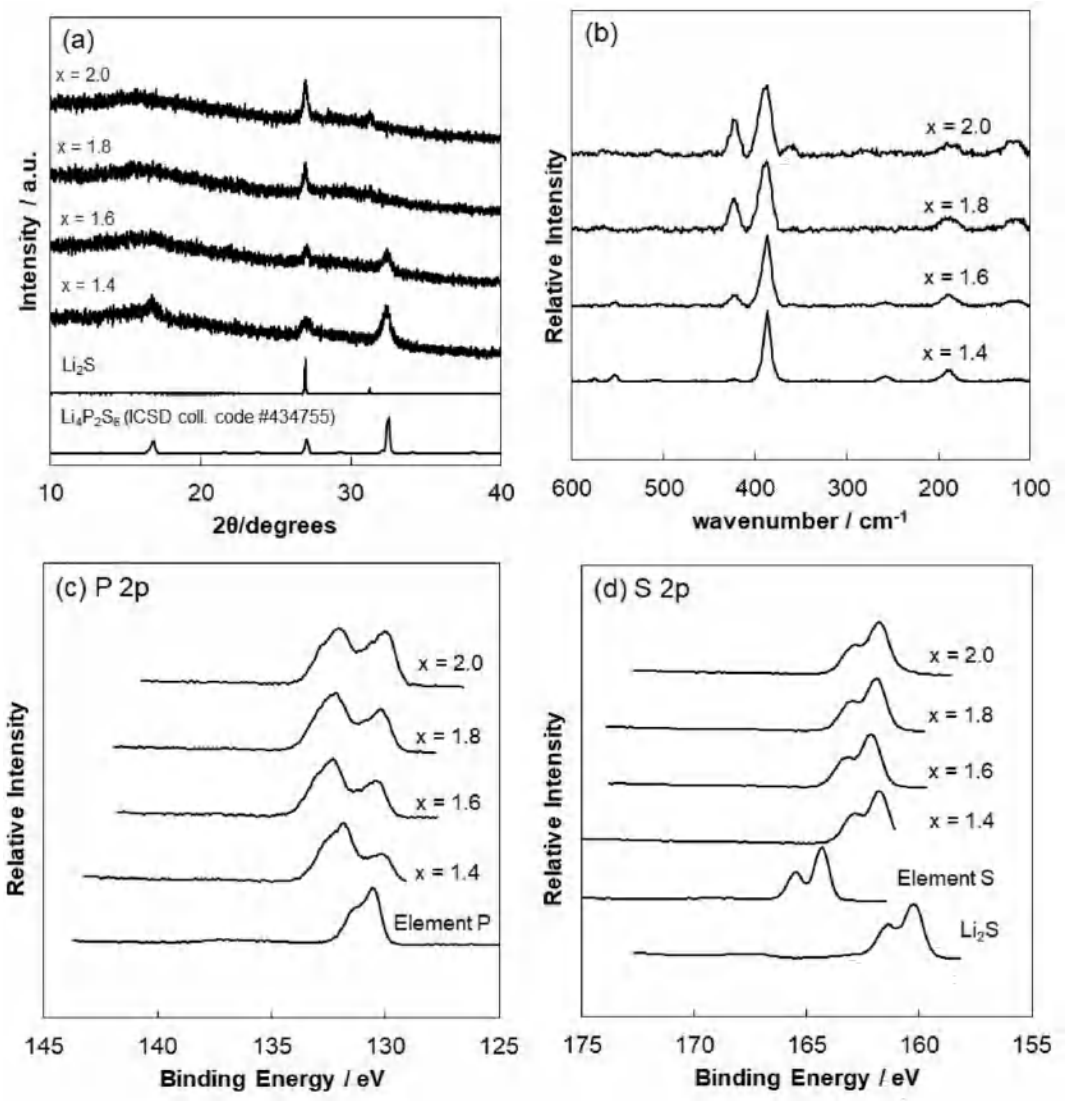

Fig. 1. XRD patterns (a) and Raman spectra (b) of Li_xPS_2 (x = 1.4, 1.6, 1.8, and 2.0). XPS spectra of P 2p (c) and S 2p (d) of Li_xPS_2 (x = 1.4, 1.6, 1.8, and 2.0) and that starting materials.

significantly varies depending on the sulfur content in the positive electrode, electrode loading weight (or electrode thickness), and current density. Therefore, it is difficult to determine which is better property. For instance, in our previous research on an all-solid-state Li–S battery [8], the thin electrode with a loading weight of 1.5 mg cm−2 and a sulfur content of 50% showed an extremely high specific capacity of 1760 mA h g−1 (sulfur) after 1000 cycles at 1.3 mA cm−2 (1C) and 25 °C by improving sulfur reactivity, but the calculated energy density of the battery was less than half that of the electrode with a loading weight of 8.3 mg cm−2. Furthermore, it is difficult to compare solid and liquid systems, because liquid systems do not consider the weight of the liquid electrolyte contained in the positive electrode. Thus, liquid systems may be perceived as having better properties than solid systems. Hence, it is necessary to carefully check the electrode formations (sulfur loading weight, sulfur content, and voidage) and the test conditions when comparing the battery performance of different positive electrodes.

In previous research, we observed a correlation between the sulfur reactivity and the P/S ratio (the number of P atoms/the number of S atoms) of the sulfide SE in the positive composite electrode and that the effect of sulfur reactivity was much higher than the influence of electronic and ionic conductivity of SEs in the positive composite electrode [9,10]. In other studies, it has been reported that ionic conductivity is significantly improved through the addition of LiI to Li_2S–P_2S_5 (LPS) [11,12]. In this study, we investigated the SEs with high sulfur activated properties and high ion conductivity through the addition of LiI to high P/S ratio SEs and evaluated the battery performance of the positive composite electrodes containing SEs in the manufacture of an all-solid-state Li–S battery.

2. Experimental

Reagent grade Li_2S (Mitsuwa Chem., 99.9%), P_2S_5 (Aldrich, 99%), sulfur (Aldrich, 99.5%), phosphorus red (Aldrich, 99.99%), and LiI (Aldrich, 99.999%) were used as the starting materials for preparing high P/S ratio SEs. The reagent sulfur was purified by sublimation before preparation. This study deals with Li_xPS_2 systems (x = 1.4, 1.6, 1.8, and 2.0) as high P/S ratio SEs. These SEs were prepared with a mechanochemical method using a planetary ball mill apparatus (Premium Line P-7, Fritsch Co.) [13]. The mechanochemical treatment using a ZrO_2 pot and 4 mm diameter ZrO_2 balls under Ar atmosphere was performed for mixing Li_2S, phosphorus red, and sulfur (molar ratios = 0.7:1.0:1.3, 0.8:1.0:1.2, 0.9:1.0:1.1, and 1.0:1.0:1.0) for 10 h. The composite SEs of high P/S ratio SEs and LiI, (100 − x) $(Li_{1.6}PS_2)$·x (LiI) (x = 0, 17, 25, 35, 44, and 54), were obtained with the mechanochemical method [14].

Reagent grade lithium iodide (Aldrich, 99.999%) and prepared $Li_{1.6}PS_2$ were used as starting materials for the LiI composite high P/S ratio SEs. (100− x) ($Li_{1.6}PS_2$)·x (LiI) was prepared using the same mechanochemical treatment in Li_xPS_2 preparation for mixing LiI and $Li_{1.6}PS_2$ (molar ratios = 0:100, 17:83, 25:75, 35:65, 44:56, and 54:46).

X-ray diffraction (XRD, Cu Kα1) was employed to identify the crystalline phases of the SEs (measured by SmartLab II, Rigaku Co.). The XRD measurement was performed using a closed cell assembled in an Ar-filled glove box to evaluate under Ar atmosphere. The Raman spectra of SEs were measured using a spectrometer (NRS-7100, JASCO Co.) with an excitation wavelength of 532 nm at 0.5 mW. The measurement sample for Raman spectroscopy, sandwiched between glass and sealed by polyimide tape, was prepared in an Ar-filled glove box to avoid contact with moisture in the air. The X-ray photoelectron spectroscopy (XPS) analyses of SEs were performed on a spectrometer (KRATOS Nova, KRATOS ANALYTICAL), using a monochromatic Al–Kα source. These binding energies were calibrated using C 1s peak at 285 eV. The measurement sample of XPS was prepared in an Ar-filled glove box and insert to the spectrometer by unexposed transporter to avoid reaction of SE and moisture in the air. The ionic conductivities of the SEs at 25 °C were calculated by AC impedance data that were collected using impedance analyzer (1260A Frequency Response Analyzer, Solartron Analytical) with an applied AC voltage of 50 mV and the range of 1–32 MHz. The 1-mm diameter pellet samples of SEs used to measure impedance were prepared by the uniaxial press at 200 MPa in an Ar-filled glove box. Then, the resulting pellet was sandwiched by two stainless steel rods acting as current collectors and placed in a sealed vessel in an Ar-filled glove box to evaluate the ionic conductivity under the Ar atmosphere.

Several positive composite electrode materials containing elemental sulfur as an active material, activated carbon (AC; Kansai Coke and Chemicals Co., Ltd.) as an electrical conducting material, and SEs were prepared by planetary ball mill apparatus under Ar atmosphere [15]. The weight ratio of the positive composite material was sulfur:AC:SE = 50:10:40. The charge–discharge performance of the positive composite electrodes was investigated in an all-solid-state cell [15]. The cell structure was a positive composite electrode/blended SE of crystalline $Li_{10}GeP_2S_{12}$ [4] and $80Li_2S–20P_2S_5$ glass [16] (B-SE) as the solid electrolyte layer/Li–In alloys as the negative electrode. Here, B-SE improved the moldability of the SE layer by 10% blending of high deformable $80Li_2S–20P_2S_5$ glass to crystalline $Li_{10}GeP_2S_{12}$ and shows high ionic conductivity of about 5 mS cm−1. Therefore, it is appropriate as a solid electrolyte layer for high rate performance evaluation of battery. 7.5 mg of the positive electrode powder and 80 mg of B-SE powder was placed in a 10-mm diameter polycarbonate tube and pressed under 200 MPa by stainless steel to form a two-layered pellet [9]. The negative electrode of Li–In alloy was formed by pressed under 80 MPa of that the stacking Li foil and In foil on the surface of the two-layered pellet in contact with the SE [9]. The resulting three-layered pellet was then sandwiched between two stainless steel rods, which acted as current collectors [9]. The molar ratio of Li/In in the negative electrode was 0.64. When x of Li_x–In was less than 1, the potential of the Li–In alloys exhibited a constant value of approximately 0.6 V vs. Li [17]. Here, the test cell was assembled in an Ar-filled glove box and placed in a sealed vessel to evaluate the battery performance under the Ar atmosphere. The battery performance of the positive composite electrodes using several (100 − x) ($Li_{1.6}PS_2$)·x (LiI) was evaluated at constant current densities ranging from 0.64 to 6.4 mA cm−2 at 25 °C and 0.64–26 mA cm−2 at 45 °C using a charge–discharge measuring device (ACD-01, Asuka Electronics Co. Ltd.).

3. Results and discussion

The XRD pattern of the Li_xPS_2 systems (x = 1.4, 1.6, 1.8, and 2.0) prepared by mechanochemical treatment is shown in Fig. 1a. Weak peaks were observed in all samples. The $Li_4P_2S_6$ phase [18] was observed at x = 1.4 and 1.6, and decreased with x. The small amount of excess Li_2S crystal phase was observed at over x = 1.8 and increased with x. Fig. 1b shows the Raman spectra of these SEs, where each spectrum is expressed in relative intensity. The main peak of all SEs was observed at around 380 cm−1 according to P_2S_6−4 [19,20]. The peak relative intensity of 420 cm−1 according to PS_4−3 increased with increasing x. It is considered that excess Li_2S reacts with $Li_4P_2S_6$ to generate Li_3PS_4. Furthermore, unidentified complicated peaks that are assumed to other lithium polysulfides also increased around 200 and 130 cm−1 [21]. The result of the Raman spectra showed that the P_2S_6−4 unit decreased with increasing x, similar to XRD. Furthermore, XPS spectra of SEs shown in Fig. 1c and d, where each spectrum is expressed in relative intensity. These P 2p XPS spectra of SEs were observed two broad peaks at around 130 and 132 eV in Fig. 1c, each peak including P $2p_{3/2}$ and $2p_{1/2}$. The broad peak of around 132 eV was assumed to several kinds of lithium phosphorus sulfides [22]. These electronic densities of these phosphorus are higher than P_2S_5 which have 133 eV of $2p_{3/2}$ binding energy, therefore, this phosphorus consider having some P–S− components, such as Li_3PS_4 and $Li_4P_2S_6$. And then, the peak of around 130 eV was assumed to elemental phosphorus. These peaks of around 130 eV of the SEs increased with increasing x, as shown in Fig. 1c. Therefore, the amount of elemental phosphorus increased with increasing x. On the other hands, these S 2p XPS spectra of SEs were observed broad peak of around 162 eV and around 163 eV in Fig. 1d, it was assumed $2p_{3/2}$ and $2p_{1/2}$ of several kinds of P–S− and P–S components [22]. In the SEs at X = 1.8 and 2.0, it considered that Li_2S is slightly included since there is the slight peak of 160 eV. All these S 2p spectra of SEs have no significant peaks of elemental sulfur. Hence, it considered that almost the excess elemental sulfur and Li_2S reacted to be lithium polysulfides. Therefore, it is assumed the exist of several lithium polysulfides and unreacted phosphorus in these SEs on the individual amount.

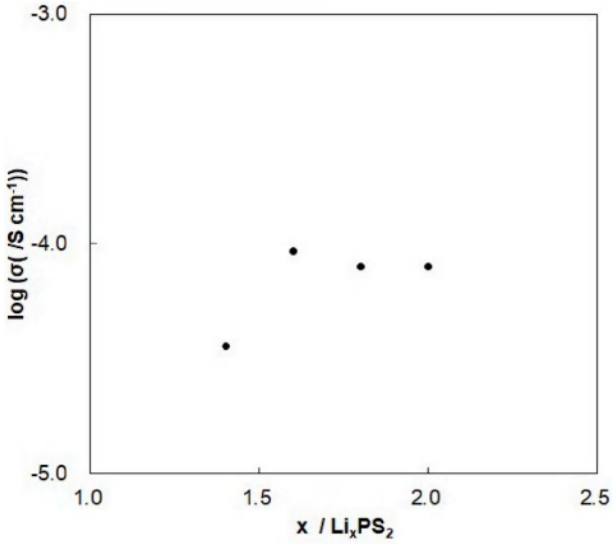

Fig. 2. Ionic conductivity of Li_xPS_2 (x = 1.4, 1.6, 1.8, and 2.0).

The conductivities of the Li_xPS_2 (x = 1.4, 1.6, 1.8, and 2.0) SEs at 25 °C are shown in Fig. 2. The conductivity of the SEs increased with increasing x until x = 1.6 and then decreased at x = 1.8 and 2.0. The composition formula of $Li_{1.6}PS_2$ showed the highest conductivity of 0.09 mS cm^{-1} in the Li_xPS_2 system. Therefore, in this study, we investigated the composite SE of LiI and $Li_{1.6}PS_2$ to improve the ionic conductivity of a high P/S ratio SE.

Fig. 3a shows the XRD pattern of the (100− x) ($Li_{1.6}PS_2$)·x (LiI) systems of x = 0, 17, 25, 35, 44, and 54. At a range of x = 17 to 44, no peaks could be found, and the excess LiI phase [23] was observed at x = 54. (100 − x) ($Li_{1.6}PS_2$)·x (LiI) became amorphous by adding LiI until x = 44. The Raman spectra of these SEs are shown in Fig. 3b. All SEs

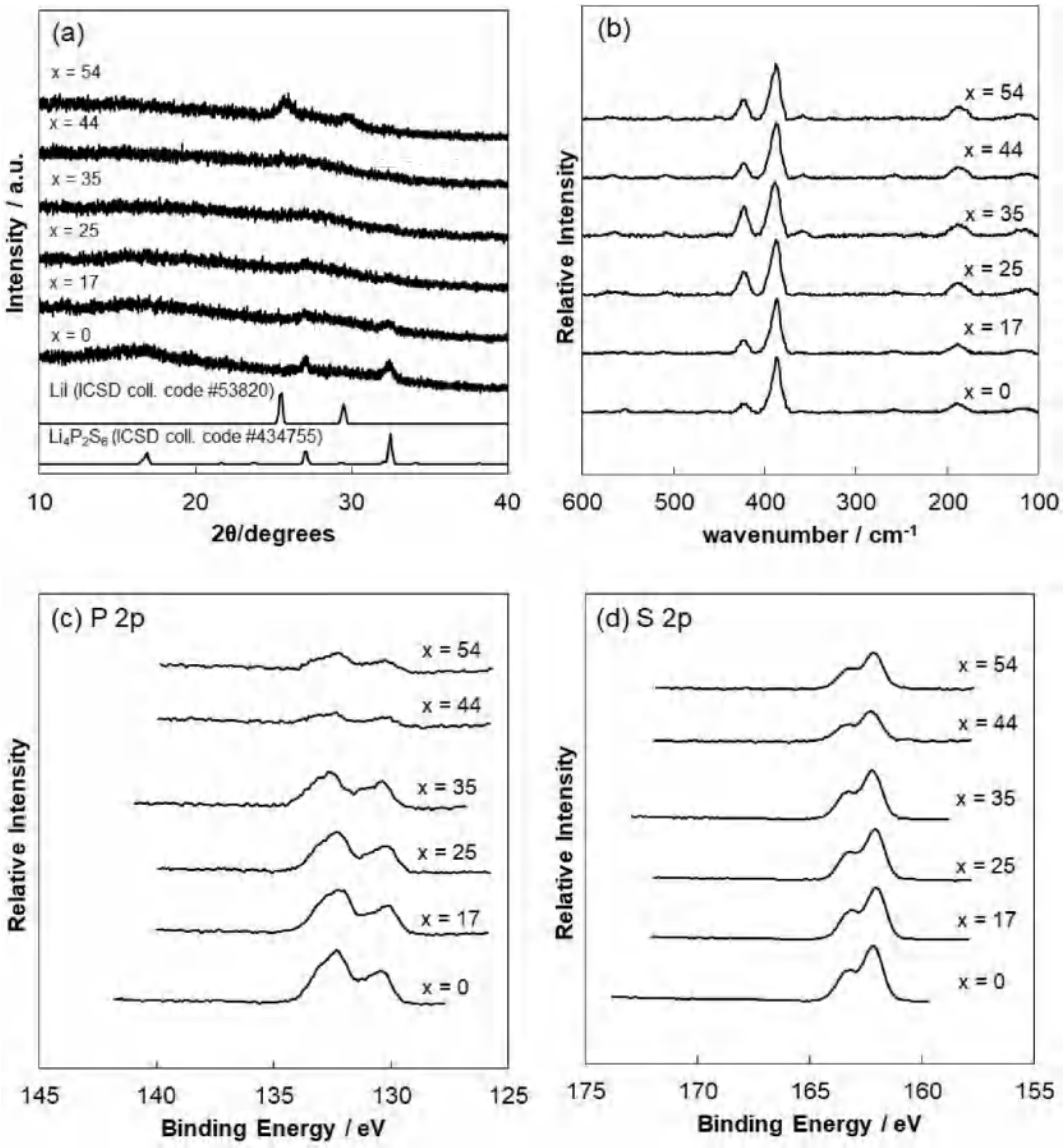

Fig. 3. XRD patterns (a) and Raman spectra (b) of (100− x) ($Li_{1.6}PS_2$)·x (LiI) (x = 0, 17, 25, 35, 44, and 54). XPS spectra of P 2p (c) and S 2p (d) of (100− x) ($Li_{1.6}PS_2$)·x (LiI) (x = 0, 17, 25, 35, 44, and 54).

showed similar spectra of original $Li_{1.6}PS_2$ having a main peak of 380 cm−1 according to P_2S_6−4. Therefore, $Li_4P_2S_6$ was considered to be the main component of the SEs. However, the peak relative intensity of 420 cm^{-1} increased compared to original $Li_{1.6}PS_2$. It considered that the reaction of excess lithium polysulfides and $Li_4P_2S_6$ would proceed to generate Li_3PS_4 by further mechanochemical treatment. Fig. 3c and d shows XPS spectra of P 2p and S 2s for SEs. Both spectra of P 2p and S 2p did not significantly change from the original $Li_{1.6}PS_2$, as shown in Fig. 3 and d. Therefore, it considered that the state of P and S in SEs did not significantly change from original $Li_{1.6}PS_2$. However, it considered the amount of $Li_4P_2S_6$ and Li_3PS_4 components were different to original $Li_{1.6}PS_2$, according to Raman spectra of SEs. The conductivities of the (100− x) ($Li_{1.6}PS_2$)·x (LiI) (x = 0, 17, 25, 35, 44, and 54) SEs at 25 °C are shown in Fig. 4. The conductivity of the SEs increased with increasing x until x = 54. At x = 0.35, 65$Li_{1.6}PS_2$–35LiI showed a high conductivity of over 0.5 mS cm^{-1}, which was the same value as 80Li_2S–20P_2S_5 glass, as a high conductivity glass SE. At x = 54, 46$Li_{1.6}PS_2$–54LiI showed a high conductivity of 0.9 mS cm^{-1}, which was 10 times higher than the original $Li_{1.6}PS_2$. For this reason, it was expected that the positive composite electrode containing (100− x) ($Li_{1.6}PS_2$)·x (LiI) would exhibit high battery performance, as it is assumed that SEs improve sulfur reactivity and ionic conductivity in positive electrodes simultaneously.

Fig. 5a and b shows charge–discharge curves at different scales where the test conditions were 0.64 mA cm^{-2} constant current charge–discharge at 25 °C and 0.5–2.5 V (*vs.* Li–In) for the all-solid-state Li–S cell prepared using several positive composite electrodes. The positive composite electrodes contained SEs of (100− x) ($Li_{1.6}PS_2$)·x (LiI) (x = 0, 17, 25, 35, and 44). All the positive composite electrodes containing (100− x) ($Li_{1.6}PS_2$)·x (LiI) exhibited a higher capacity and discharge potential during the whole discharge process than those containing $Li_4PS_{4.5}$. This is assumed to be the effect of high sulfur activated effect owing to the high P/S ratio of (100−x) ($Li_{1.6}PS_2$)·x (LiI). There was a significant tendency for the capacity over 0.6V, corresponding to sulfur redox, to increase with increasing x, and for the capacity under 0.6V, corresponding to P/S compounds redox, to decrease. These results suggest that a decreasing high P/S ratio SE amount with increasing LiI amount in SEs decreases the reaction of SE and sulfur active materials, similar to the findings of previous research [9]. Here, the sulfur reactivity of these positive composite electrodes is based on the early period discharge potential of the all-solid-state Li–S battery, which mainly corresponds to sulfur reactivity because the Li-ion transfer distance is short in that period. However, the mechanism for improving the sulfur

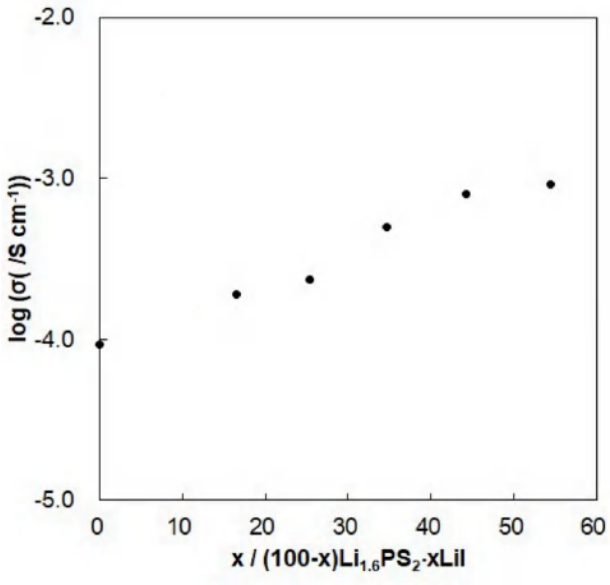

Fig. 4. Ionic conductivity of (100− x) ($Li_{1.6}PS_2$)·x (LiI) (x = 0, 17, 25, 35, 44, and 54).

reactivity has not been clarified. Here, Fig. 5c and d shows XPS spectra of positive composite electrode using $65Li_{1.6}PS_2{\cdot}35LiI$ and that starting materials. The peak of around 130 eV which assumed to excess element P decreased in the positive composite electrode and considered to generate lithium phosphorus sulfides, as shown in Fig. 5c. Then, the broad peak of 133 eV which assumed P–S− and P–S components was slightly changed to higher binding energy form starting material of $65Li_{1.6}PS_2{\cdot}35LiI$ [22]. It suggests that electronic density of phosphorus is decreased by reaction of $65Li_{1.6}PS_2{\cdot}35LiI$ and element sulfur. Therefore, it considered that the amount of P–S− component was decreased and P–S component was increased. On the other hands, the peak of around 164 eV which assumed to S^0 of S–S component in the positive composite electrode was slightly changed to lower binding energy form element sulfur, as shown in Fig. 5d. Hence, it considered that a part of sulfur active material reacted with lithium phosphorus sulfide such as $Li_4P_2S_6$ and excess element P by mechanochemical treatment. Therefore, we speculate that the dissociation property of the S–S bond in the P-S_x chain resulting from the reaction of $Li_4P_2S_6$ and excess element P with S_8 is improved. These early period discharge potentials exhibited a close value at x = 0 to 35, and a lower value at x = 44, as shown in Fig. 5b. It is assumed that the sulfur reactivity decreased with increasing LiI because the high P/S ratio SE affected the sulfur reactivity. In addition, the ionic conductivity also affected the discharge potentials. Therefore, until x = 35, it is proposed that the contribution of the ion conductivity improvement effect is greater than the decrease in the sulfur reactivity improvement effect.

Fig. 6a shows the discharge rate performance of the positive composite electrodes at 25 °C (cut off voltage 0.5 V *vs.* Li–In). The rate performances was measured under several discharge current densities of 0.64, 1.3, 3.2, and 6.4, mA cm^{-2} after 0.64 mA cm^{-2} CC−CV full charge (cut off voltage of charge is 2.5 V *vs.* Li–In). A low rate discharge

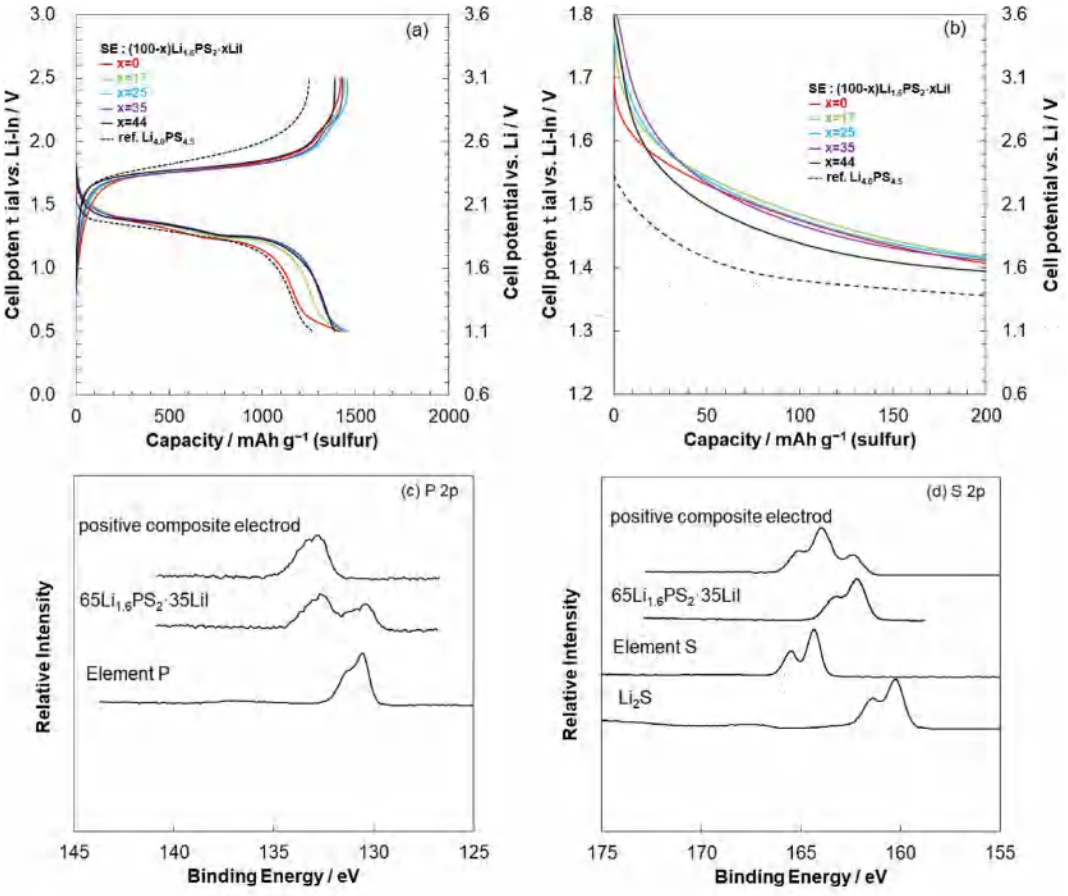

Fig. 5. Charge–discharge curves (a) and early period discharge curves (b) of the all-solid-state Li–S cells with positive composite electrodes containing (100− x) ($Li_{1.6}PS_2$)·x (LiI) solid electrolytes under 0.64 mA cm−2 at 25 °C. (x = 0: red line, x = 17: green line, x = 25: blue line, x = 35: purple line, x = 44: black line, and reference $Li_{4.0}PS_{4.5}$: dotted line). XPS spectra of P 2p (c) and S 2p (d) of positive composite electrode using $65Li_{1.6}PS_2{\cdot}35LiI$ and that starting materials. (For interpretation of the references to colour in this figure legend, the reader is referred to the Web version of this article.)

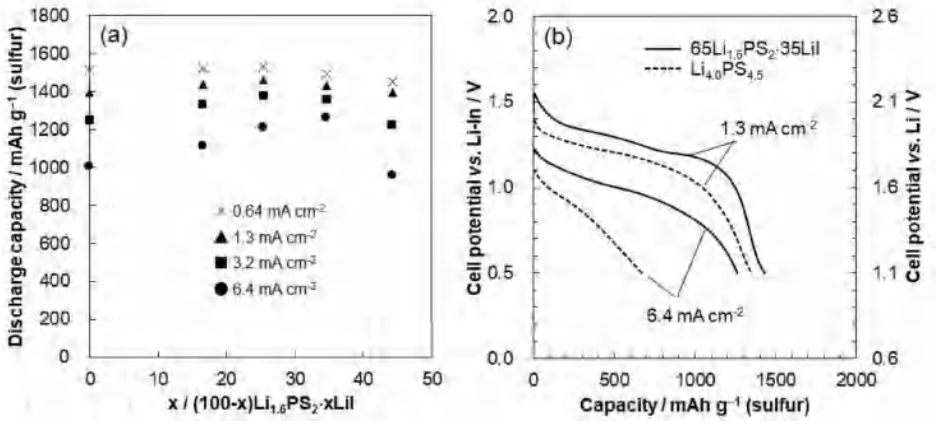

Fig. 6. Plots of discharge capacity of the all-solid-state Li–S cells with positive composite electrodes containing (100− x) ($Li_{1.6}PS_2$)·x (LiI) under several discharge current densities at 25 °C (a), discharge curves of x = 35 (solid line) and reference $Li_{4.0}PS_{4.5}$ (dotted line) under 1.3 and 6.4 mA cm−2 at 25 °C (b).

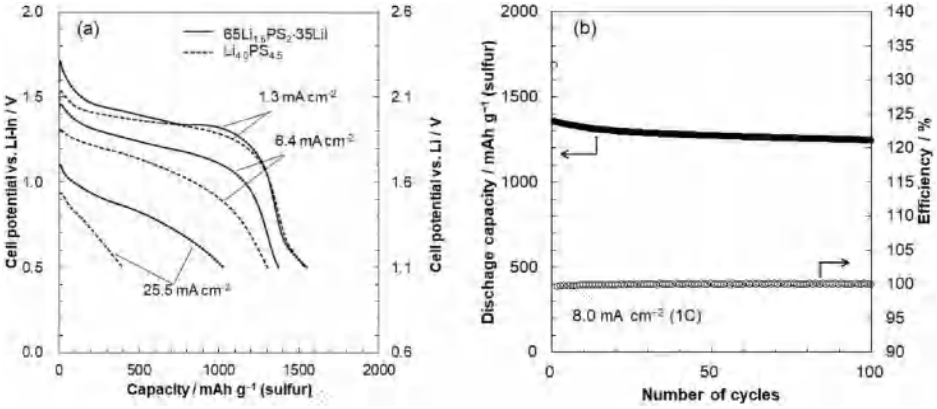

Fig. 7. Discharge curves of the all-solid-state Li–S cells with positive composite electrodes containing $65Li_{1.6}PS_2$·35LiI (solid line) and reference $Li_{4.0}PS_{4.5}$ (dotted line) under 1.3, 6.4, and 25.5 mA cm−2 at 45 °C (a). Cycling performance of all-solid-state Li–S cells with positive composite electrodes containing $65Li_{1.6}PS_2$·35LiI under 8.0 mA cm−2 CC–CV charge (CV 1 h) and 8.0 mA cm^{-2} CC discharge at 45 °C (b).

capacity at 0.64 mA cm^{-2} increased with increasing x of (100− x) ($Li_{1.6}PS_2$)·x (LiI) using a positive composite electrode until x = 25. Over x = 35, the capacity decreased with increasing x, because the capacity of under 0.6 V (*vs.* Li–In) was high when x was small. On the other hand, the high rate discharge capacity of 6.4 mA cm^{-2} increased with increasing x of (100− x) ($Li_{1.6}PS_2$)·x (LiI) until x = 35. In the test conditions of high current densities, the capacity component of under 0.6 V (*vs.* Li–In), which is considered PS compounds, is not obtained at measurement voltage range of 2.5–0.5 V (*vs.* Li–In) because the overall discharge potentials were decreased. Therefore, the capacity at a lower x of (100 − x) ($Li_{1.6}PS_2$)·x (LiI) was lower than at x = 35, despite the similar reactivity, as shown in Fig. 6b. It is proposed that the ionic conductivity of the SEs significantly affected the high rate discharge performance as the positive composite electrodes had similar sulfur reactivity until x = 35, and the ionic conductivity of SEs increased with increasing LiI, as discussed above in Figs. 5b and 4. Similarly, at over x = 44, the capacity suddenly decreased, corresponding to the lower sulfur reactivity, as discussed in Fig. 5b. Fig. 6b shows the high rate discharge curves of the positive composite electrodes containing $65Li_{1.6}PS_2$·35LiI and $Li_4PS_{4.5}$ at 25 °C. The positive composite electrode containing $65Li_{1.6}PS_2$·35LiI at 6.4 mA cm^{-2} showed an extremely high capacity of 1260 mA h g^{-1} that was over two times higher than $Li_4PS_{4.5}$. The whole high rate discharge potential of the positive composite electrode was high, and the voltage drop in the late stage of discharge was also small. This indicates that the positive composite electrode containing $65Li_{1.6}PS_2$·35LiI had high sulfur reactivity and ionic conductivity. Therefore, a composite SE with a high P/S ratio lithium phosphorus sulfide and LiI was shown to be a very effective means of improving high rate battery performance.

Finally, the changes in the charge–discharge performances according to temperature were evaluated. Fig. 7a shows the high rate performance of the positive composite electrodes containing $65Li_{1.6}PS_2$·35LiI at 45 °C (cut off voltage is 0.5 V *vs.* Li–In). The rate performances at 45 °C was measured under several discharge current densities of 1.3, 6.4, and 25.5 mA cm^{-2} after 0.64 mA cm^{-2} CC−CV full charge (cut off voltage of charge is 2.5 V *vs.* Li–In). At 6.4 mA cm^{-2}, the discharge capacity showed 1370 mA h g^{-1}. Furthermore, the discharge curve indicated 250 mV higher potentials than at 25 °C. This indicated that the positive composite electrode containing $65Li_{1.6}PS_2$·35LiI improved as the temperature increased. Moreover, IR drops of the positive composite electrode containing $65Li_{1.6}PS_2$·35LiI with increasing discharge current densities were smaller than those containing $Li_4PS_{4.5}$. This suggests that the activation energy of the positive composite electrode containing $65Li_{1.6}PS_2$·35LiI was much lower than those containing $Li_4PS_{4.5}$. These results correspond to the early period discharge potentials in Fig. 5b, which can be considered a sulfur reactivity evaluation index.

Fig. 7b shows the cycling properties of the positive composite electrode containing $65Li_{1.6}PS_2$·35LiI at 8.0 mA cm^{-2} and 45 °C, where the cycle test conditions were 8.0 mA cm^{-2} (1C) CC−CV (CV 1h) charge and 8.0 mA cm^{-2} (1C) CC discharge. The first discharge capacity showed 1350 mA h g^{-1} and maintained discharge capacity of over 1230 mA h g^{-1} after 100 cycles. The coulombic efficiency was almost 100% during

100 cycles except for the first cycle. The first charge capacity exhibit lower than second cycle because the cycle test was performed after rate performance test (after 25.5 mA cm^{-2} discharge test at 45 °C). The decrease in cycle discharge capacities were caused by the decrease in charge capacity on each cycle. The battery performance of the positive composite electrode was significantly higher than other Li–S battery systems, in spite of the high sulfur content, high loading weight, and high current density [7]. Here, we propose very simple calculation method for evaluating energy density of positive electrode. First, it will define that the positive electrode is placed on 10 μm of Al current collector (density is 2.7 g cm^{-3}). So, weight per unit area of the positive electrode is sum of loading weight of the positive composite electrode and Al current collector weight (2.7 mg cm^{-2}). Then, energy densities of positive electrode at several current densities are obtained by normalizing the product of the average discharge potential (vs. Li) and the capacity by the positive electrode weight. This calculation method can consider the influence of sulfur loading weight and content. Furthermore, by including the weight of the liquid electrolyte in the positive electrode, it is suitable for battery performance evaluation of liquid type electrodes. Using this method, the energy density of the positive composite electrode containing $65Li_{1.6}PS_2{\cdot}35LiI$ at 1.3 mA cm^{-2} and 25 °C, 6.4 mA cm^{-2} and 25 °C, and 25.5 mA cm^{-2} and 45 °C exhibit 990, 740, and 560 Wh kg^{-1}, respectively. Thus, using this positive composite electrode for an all-solid-state Li–S battery is expected to produce a much high energy density battery.

4. Conclusions

The all-solid-state Li–S batteries exhibited improvement in the battery performance of a positive composite electrode by using a composite SE with high P/S ratio lithium phosphorus sulfide and LiI. The composite SEs had high ionic conductivity and improved the sulfur reactivity of the positive composite electrode by high P/S ratio SE. The addition of LiI to high P/S ratio lithium phosphorus sulfide was effective in improving the ionic conductivity, and the composite SE of $65Li_{1.6}PS_2{\cdot}35LiI$ showed a high P/S ratio of 0.5 and a high ionic conductivity of 0.5 mS cm^{-1}. The positive composite electrode containing $65Li_{1.6}PS_2{\cdot}35LiI$ showed an excellent high rate performance of over 1260 mA h g^{-1} (sulfur) at 6.4 mA cm^{-2} (0.8 C) and 25 °C and over 1000 mA h g^{-1} at 25.5 mA cm^{-2} (3.2 C) and 45 °C. Furthermore, it showed good cycle performance, with an 8.0 mA cm^{-2} (1 C) cycle capacity of over 1230 mA h g^{-1} after 100 cycles.

Declaration of competing interest

The authors declare that they have no known competing financial interests or personal relationships that could have appeared to influence the work reported in this paper.

CRediT authorship contribution statement

Hiroshi Nagata: Conceptualization, Methodology, Investigation, Writing - review & editing. **Yasuo Chikusa:** Conceptualization, Methodology. **Junji Akimoto:** Supervision, Writing - review & editing.

References

[1] X. Ji, L.F. Nazar, J. Mater. Chem. 20 (2010) 9821–9826.
[2] B.H. Jeon, J.H. Yeon, K.M. Kim, I.J. Chung, J. Power Sources 109 (2002) 89–97.
[3] M. Nagao, A. Hayashi, M. Tatsumisago, Electrochim. Acta 56 (2011) 6055–6059.
[4] N. Kamaya, K. Homma, Y. Yamakawa, M. Hirayama, R. Kanno, M. Yonemura, T. Kamiyama, Y. Kato, S. Hama, K. Kawamoto, A. Mitsui, Nat. Mater. 10 (2011) 682–686.
[5] Y. Kato1, S. Hori, T. Saito, K. Suzuki, M. Hirayama, A. Mitsui, M. Yonemura, H. Iba, R. Kanno, Nature Energy 1 (4) (2016) 16030.
[6] L. Yuan, J. Feng, X. Ai, Y. Cao, S. Chen, H. Yang, Electrochem. Commun. 8 (2006) 610–614.
[7] X. Judez, H. Zhang, C. Li, G.G. Eshetu, J.A. González-Marcos, M. Armand, L. M. Rodriguez-Martineza, J. Electrochem. Soc. 165 (1) (2018) A6008–A6016.
[8] H. Nagata, Y. Chikusa, Energy Technol. 4 (2016) 484–489.
[9] H. Nagata, Y. Chikusa, J. Power Sources 263 (2014) 141–144.
[10] H. Nagata, Y. Chikusa, Energy Technol. 2 (2014) 753–756.
[11] R. Mercier, J.P. Malugani, B. Fahys, G. Robert, Solid State Ionics 5 (1981) 663–666.
[12] H. Nagata, Y. Chikusa, J. Power Sources 329 (2016) 268–272.
[13] T. Ohtomo, F. Mizuno, A. Hayashi, K. Tadanaga, M. Tatsumisago, Solid State Ionics 176 (2005) 2349–2353.
[14] S. Ujiie, T. Inagaki, A. Hayashi, M. Tatsumisago, Solid State Ionics 263 (2014) 57–61.
[15] M. Nagao, A. Hayashi, M. Tatsumisago, Electrochim. Acta 56 (2011) 6055–6059.
[16] A. Hayashi, S. Hama, T. Minami, M. Tatsumisago, Electrochem. Commun. 5 (2003) 111–114.
[17] K. Takada, N. Aotani, K. Iwamoto, S. Kondo, Solid State Ionics 86 (1996) 877–882.
[18] S. Neuberger, S.P. Culver, H. Eckert, W.G. Zeier, J. Schmedt Auf Der Günne, Dalt. Trans. 47 (2018) 11691–11695.
[19] M. Tachez, J.P. Malugani, R. Mercier, G. Robert, Solid State Ionics 14 (1984) 181–185.
[20] C. Dietrich, D.A. Weber, S.J. Sedlmaier, S. Indris, S.P. Culver, D. Walter, J. Janek, W.G. Zeier, J. Mater. Chem. A. 5 (2017) 18111–18119.
[21] W. Chen, T. Lei, T. Qian, W. Lv, W. He, C. Wu, X. Liu, J. Liu, B. Chen, C. Yan, J. Xiong, Adv. Energy Mater. 8 (2018) 1702889.
[22] C. Dietrich, R. Koerver, M.W. Gaultois, G. Kieslich, G. Cibin, J. Janek, W.G. Zeier, Phys. Chem. Chem. Phys. 20 (2018) 20088–20095.
[23] E. Posnjak, R.W.G. Wyckoff, J. Wash. Acad. Sci. 12 (1922) 248–251.